

# Stochastic Acceleration in the Western Hotspot of Pictor A

Zhong-Hui Fan<sup>1</sup>, Siming Liu<sup>2</sup>, Jian-Min Wang<sup>1</sup>, Christopher L. Fryer,<sup>2,3</sup> and Hui Li<sup>2</sup>

## ABSTRACT

*Chandra's* high resolution observations of radio galaxies require a revisit of the relevant electron acceleration processes. Although the diffusive shock particle acceleration model may explain spectra of spatially unresolved sources, it encounters difficulties in explaining the structure and spectral properties of recently discovered *Chandra* X-ray features in several low-power radio sources. We argue that these observations strongly suggest stochastic electron acceleration by magnetized turbulence, and show that the simplest stochastic particle acceleration model with energy independent acceleration and escape timescales can overcome most of these difficulties. We use the bright core of the western hotspot of Pictor A as an example to demonstrate the model characteristics, which may be tested with high energy observations.

*Subject headings:* acceleration of particles — galaxies: individual (Pictor A) — galaxies: jets — radiation mechanisms: non-thermal

## 1. Introduction

In the classical diffusive shock particle acceleration model the observed relativistic electrons in radio galaxies are accelerated at the edges and knots of jets. For relatively more luminous FR II radio galaxies, electrons may also be energized in radio hotspots, where jets terminate. It is usually assumed that the jet power is initially stored in the bulk motion of outflows and is converted into the internal energy of the jet plasma by shocks at the observed radio bright features (Blandford & Rees 1974). The model requires that particles repeatedly pass the shock front, characterized by a jump in the density and velocity field, to reach very high energies. Although the physical processes responsible for the scattering and/or diffusion

---

<sup>1</sup>Key Laboratory for Particle Astrophysics, Institute of High Energy Physics, Chinese Academy of Sciences, 19B Yuquan Road, 100049 Beijing, China; zxfan@ihep.ac.cn, wangjm@ihep.ac.cn

<sup>2</sup>Los Alamos National Laboratory, Los Alamos, NM 87545; liusm@lanl.gov, hli@lanl.gov

<sup>3</sup>Physics Department, The University of Arizona, Tucson, AZ 85721; clfreyer@lanl.gov

of particles through the shock front in most collisionless astrophysical plasmas are not well established, it has been widely cited due to its simplicity and its achievement in explaining the spectra of spatial unresolved sources (e.g. Hardcastle et al. 2001).

It however is challenged by recent high spatial and spectral resolution observations with *Chandra*. Although nonthermal X-rays from radio galaxies can be produced by relativistic electrons through synchrotron, synchrotron self-Comptonization (SSC), and inverse Compton scattering of the cosmic microwave background radiation (CMBR) or other background photons, X-rays from jets of FR I galaxies and some low-power hotspots of FR II galaxies are generally attributed to synchrotron process (Worrall, Birkinshaw, & Hardcastle 2001; Hardcastle et al. 2004). If the magnetic field is nearly in energy equipartition with the relativistic electrons, the synchrotron cooling timescale of electrons producing the observed X-rays is short, and the electrons need to be accelerated very close to the observed compact X-ray features, which usually are displaced from peaks of the corresponding radio sources and occasionally do not have optical and/or radio counterparts (Hardcastle et al. 2001, 2007a; Marshall et al. 2002; Wilson & Young 2002). The diffuse X-ray emission from jets of FR I galaxies, on the other hand, indicates a distributed particle acceleration process. The X-ray spectral hardening and relatively high X-ray flux as compared to the extrapolation from optical fluxes of some compact sources are also puzzling.

The bright core of the western hotspot of Pictor A (WHPA), a famous nearby<sup>1</sup> FR II galaxy, is an excellent candidate to demonstrate difficulties of the shock model. Meisenheimer, Yates & Roepke (1997) discussed its radio to optical spectrum, and Wilson, Young & Shopbell (2001) reported X-ray observations with *Chandra*. The latter studied in detail several possible X-ray emission processes and found that none of them can explain the broadband spectrum (BBS) naturally. They concluded that the X-rays are most likely synchrotron emission by an electron population distinct from these responsible for the radio to optical spectrum. In this picture the fact that the radio, optical, and X-ray emissions come from the same spatial region would have to be a coincidence.

In this Letter, we show how the simplest stochastic particle acceleration (SA) model explains the BBS of WHPA. The model also predicts a spectral cutoff near the *Chandra* band and an intrinsic volume of  $0'.03^3$  of the particle acceleration region (AR), which may be tested with future observations. In § 2, we discuss the major difficulties of the shock model in explaining *Chandra* observations and why the SA by turbulence is favorable. A simple

---

<sup>1</sup>At a redshift of  $z = 0.035$ , the luminosity distance to Pictor A is  $d_L = 151.9$  Mpc, and the conversion scale is  $1'' = 0.687$  kpc for the modern cosmology with  $\Omega_M = 0.27$ ,  $\Omega_\Lambda = 0.73$ , and  $H_0 = 71$  km s<sup>-1</sup> Mpc<sup>-1</sup> (Spergel et al. 2003).

SA model is built and applied to WHPA in § 3. In § 4 we draw conclusions and discuss how the model may also explain other *Chandra* X-ray features.

## 2. Shock VS Stochastic Acceleration

The synchrotron cooling time of an isotropic electron population is given by  $\tau_{\text{syn}} = 9m_e^3c^5/4e^4B^2\gamma = 24.6\gamma^{-1}B^{-2}$  yr, where  $m_e$ ,  $e$ ,  $\gamma$ ,  $c$ , and  $B$  are the electron mass, charge, Lorentz factor, the speed of light, and magnetic field, respectively. Here and in what follows, c.g.s. units are adopted. The synchrotron power spectrum peaks near  $\sim 1.7 \times 10^{-11}B\gamma^2$  keV. For a 0.1 mG magnetic field, typical for jets and hotspots of radio galaxies, the X-ray emitting electrons have  $\gamma > 3 \times 10^7$  and  $\tau_{\text{syn}} < 82$  yr. The corresponding light travel distance is  $< 25$  pc, which is comparable to or smaller than the *Chandra* resolution for most radio galaxies. The X-ray emitting electrons therefore need to be accelerated near the observed X-ray sources. In the standard diffusive shock model, particles are accelerated at a thin shock front and are carried away by the shocked flow into the downstream. The simplest 1-D model predicts a power-law synchrotron spectrum that cuts off at the frequency where the synchrotron cooling time is equal to the flow travel time from the shock front (Heavens & Meisenheimer 1987). Then the spatially integrated spectrum from any segment of the downstream region can be fitted with a broken power-law, which cuts off at the cutoff frequency of the boundary closer to the shock front. The break frequency corresponds to the cutoff frequency of the farther boundary. The model has difficulties in accounting for the following *Chandra* observations:

(i) If the diffuse X-ray emission from jets is to be associated with spatially unresolved shocks, the jet dynamics must be sophisticated enough to induce many shocks. (ii) The X-ray spectral hardening is observed in a few jet knots of FR I galaxies and hotspots of FR II sources, e.g., knot WK7.8 of PKS 0637-752 (Schwartz et al. 2000), some knots in the jets of M87, 3C 120 and NGC 6251 (Wilson & Young 2002; Harris, Mossman, & Walker 2004; Sambruna et al. 2004), WHPA (Wilson, Young & Shopbell 2001), and hotspot P1/2 of 3C227 (Hardcastle et al. 2007a). Dermer & Atoyan (2002) suggested that it may be due to the Klein-Nishina effects of inverse Compton scattering of CMBR by relativistic electrons that produce the observed X-ray through synchrotron process. The model requires an extremely low magnetic field with an energy density comparable to that of the local CMBR or very strong Doppler effects and may not be applicable to most of the observed X-ray sources in radio galaxies, which are still quite powerful and do not show strong Doppler effects. The extreme hardening of hotspot P1/2 of 3C227 and inner ( $< 50'$ ) jet of Centaurus A is even more challenging. The photon spectral indexes of these sources can be as small as

1.6 corresponding to an electron spectral index of 2.2, which can not be a cooling spectrum in the shock model. The lifetime of these sources therefore must be shorter than the synchrotron cooling time of X-ray emitting electrons. Given the observed source extension, a thin shock front may not be able to accelerate enough electrons to produce the observed X-ray flux over such a short time scale ( $< 100$  yr). **(iii)** The displacement of X-ray peaks with respect to the corresponding optical and/or radio peaks (Wilson & Young 2002; Hardcastle et al. 2001). The shock model predicts that higher energy emission is produced closer to the shock front, and the distance of synchrotron emission peak from the shock front is inversely proportional to the square root of the emission frequency for a constant downstream velocity and magnetic field (Meisenheimer et al. 1989). There is no observational evidence for such a source structure. On the contrary, much more complicated structures are seen in a few low-power hotspots of FR II galaxies (Hardcastle et al. 2007a).

While radio observations are generally consistent with shock models for hotspots (Meisenheimer et al. 1989; Carilli et al. 1991), there are indications of electrons being accelerated directly by magnetic fields in giant radio galaxies (Kronberg et al. 2004). Optical detections of some of these radio sources show that electrons are accelerated in extended regions that may not be associated with shocks (Meisenheimer, Yates & Roeser 1997). Little is known about this distributed acceleration process driven by free energy dissipations. The high Reynolds numbers of the observed radio sources suggest that turbulence may mediate these dissipations and accelerate some particles, the so-called SA, a second order Fermi acceleration that has been ignored in most astrophysical situations due to its relatively lower efficiency. The observed cutoffs of synchrotron spectra suggest that the acceleration is less efficient than that given by the diffusive shock with Bohm diffusion (Brunetti et al. 2003; Hardcastle et al. 2004). Moreover, for strongly magnetized plasmas, the Alfvén velocity can be comparable to  $c$  and SA can be effective (Petrosian & Liu 2004). These combined with the *Chandra* observations strongly suggest that SA may be the dominant acceleration mechanism in radio galaxies.

SA occurs wherever there are turbulent magnetic fields and can operate over an extended region with its size dictated by the turbulence generation and decay rates. Emission from the AR therefore can be significant. We consider the simplest SA model with energy independent acceleration ( $\tau_{ac}$ ) and escape ( $\tau_{esc}$ ) times. Then the steady-state particle distribution in the AR is given by (Schlickeiser 1984; Park & Petrosian 1995; Liu, Melia & Petrosian 2006):

$$N_{ac}(\gamma) \propto \gamma^{\delta+2} \exp(-\gamma/\gamma_c) \\ \times \begin{cases} \int_0^\infty x^{\delta-1} (1+x)^{3+\delta} e^{-\gamma x/\gamma_c} dx & \text{for } \gamma > \gamma_{inj} \\ \int_0^1 x^{\delta-1} (1-x)^{3+\delta} e^{\gamma x/\gamma_c} dx & \text{for } \gamma < \gamma_{inj} \end{cases}$$

where  $\delta = (9/4 + \tau_{\text{ac}}/\tau_{\text{esc}})^{1/2} - 1.5$ ,  $\gamma_c = 9m_e^3 c^5 / 4e^4 B^2 \tau_{\text{ac}}$ , and we have assumed that electrons are injected into the AR at  $\gamma_{\text{inj}}$  and the synchrotron cooling dominates.

As in the shock model, electrons escaping the AR may produce most of the observed emission in a region dominated by cooling processes. The corresponding particle distribution at time  $t$  since the acceleration starts is given by (Blumenthal & Gould 1970)

$$N_{\text{cool}}(\gamma, t) = \int_0^t \frac{\dot{\gamma}(\gamma_0)}{\dot{\gamma}(\gamma)} \frac{N_{\text{ac}}(\gamma_0)}{\tau_{\text{esc}}} dt_0,$$

where  $\dot{\gamma}(\gamma) < 0$  is the energy loss rate and  $t_0 - t = \int_{\gamma}^{\gamma_0} d\gamma' / \dot{\gamma}(\gamma')$ . Note that if  $t_0 - t < \int_{\gamma}^{\infty} d\gamma' / \dot{\gamma}(\gamma')$ , the integrand should be set to zero. The thin dashed and dotted-dashed lines in Figure 1 give  $N_{\text{ac}}$  and  $N_{\text{cool}}$ , respectively, for  $\gamma_{\text{inj}} = 1800$ ,  $\delta = 1.48$ ,  $\gamma_c = 1.04 \times 10^7$ ,  $t = 17.9\tau_{\text{ac}}$  (see § 3 on values of these parameters) and  $\dot{\gamma} \propto -\gamma^2$ . We see that the spatially integrated particle distribution as indicated by the thin solid line is very similar to the result of the shock model, although the AR can be much more extended in the SA model.

### 3. Application to WHPA

To apply the model to hotspots of radio galaxies, one needs to take into account the effects of adiabatic expansion (Carilli et al. 1991; Brunetti et al. 2003). Such an expansion is expected since the pressures of hotspot plasmas are usually much higher than their surroundings. To simplify the model, we assume that this expansion is decoupled from the acceleration and cooling processes, i.e. the AR experiences a quick adiabatic expansion before merging into the cooling region (CR). For a spherical AR with its radius increased by a factor of  $\Delta r$  during the expansion, the magnetic field energy density decreases by a factor of  $\Delta r^4$  and the energy of relativistic electrons decreases by a factor of  $\Delta r$ . After the expansion, the plasma enters a relatively uniform cooling region. We are mostly interested in the synchrotron emission. To reproduce the optically thin synchrotron spectrum of the AR with the magnetic field of the CR, one needs to increase the electron energy and total number by a factor of  $\Delta r$  and  $\Delta r^2$ , respectively, since the synchrotron frequency and luminosity are proportional to  $B\gamma^2$  and  $B^2\gamma^2$ , respectively. The thick lines in Figure 1 show these equivalent electron distributions for  $\Delta r = 2.5$ . Emission from the adiabatic expansion phase can be ignored as far as our assumption of quick expansion withheld. We see that the overall spectrum becomes harder right below the cutoff due to dominance of the AR there.

Figure 2 shows the BBS of WHPA, where all data are taken from Wilson, Young & Shopbell (2001). To fit it with the synchrotron spectrum of the electron distribution in Figure 1, one can have a  $\Delta r > 1$  and use the hardening of the electron distribution below the cutoff to produce the observed X-ray spectral hardening. For a given  $B$ , one can constrain

$\gamma_c$  and  $\Delta r$  by fitting the X-ray spectrum. The radio spectral index  $\alpha = 0.74$  implies  $\delta = 1.48$ . Then the frequency of the synchrotron spectral break from the radio to X-ray band determines  $t$ . The intrinsic dimension of the bright core of WHPA is  $2'' \times 1'' \times 1''$  (Perley, Röser & Meisenheimer 1997), the equivalent radius  $R = 0''.78 = 1.65 \times 10^{21}$  cm. The normalization of the electron distribution is then determined by the flux density (Doppler effects are ignored here). Migliori et al. (2007) find the electron to magnetic field energy density ratio  $U_e/U_B \sim 25(\gamma_{\text{inj}}/50)^{-0.6}$  in the radio lobes of Pictor A. Since relativistic electrons and magnetic field experience the same adiabatic expansion loss from hotspots to radio lobes and the former is also subject to radiative losses, this ratio should be higher in the hotspot. We assume  $U_e/U_B = 15(\gamma_{\text{inj}}/1800)^{1-\delta}$  and adjust  $B$  to fit the BBS. The thick solid line in Figure 2 shows the corresponding best fit, where, besides the parameters discussed above,  $B = 85 \mu\text{G}$  and the electron density  $n_e = 2.8 \times 10^{-6} \text{ cm}^{-3}$  in the CR. The X-ray spectral hardening is reproduced with a  $\Delta r = 2.5$ . The lifetime of the CR  $t = 5.2 \text{ kyr}$ . The energy flux carried away by electrons and magnetic field from the AR is  $1.5 \times 10^{45} \text{ erg s}^{-1}$ , which is a reasonable low limit of the jet power. For an electron-proton plasma without a low energy component, the corresponding Alfvén velocity is  $0.26c$  implying a highly magnetized plasma.

The equivalent radius of the AR  $R_a = 4.0 \times 10^{19} \text{ cm}$ . The corresponding light crossing time of 42 yrs is much longer than the cooling time of 7.4 yr at  $\gamma_c$  (i.e. the acceleration time  $\tau_{\text{ac}}$ ) in the AR. Therefore the shock model has difficulties in reproducing the X-ray flux since the lifetime of the X-ray emitting electrons (with  $\gamma \sim \gamma_c$ ) is too short for a thin shock front to generate enough such electrons to reproduce the observed flux. One can remedy the shock model by decreasing the magnetic field in the downstream region or increasing the shock front cross section. The former requires a magnetic field energy density far below the equipartitional value with the electrons, which seems unlikely given that a strong magnetic field is required to convert the jet energy into the energy of particles. For a downstream flow velocity  $v_d$ , the latter requires a cross section greater than  $4\pi R_a^3/3v_d\tau_{\text{ac}} \simeq (0.1c/v_d)(0''.3)^2$ . From  $\delta = 1.48$ , we have  $\tau_{\text{esc}} = \tau_{\text{ac}}/6.6$ , the thickness of the AR needs to be on the order of  $1.1 \text{ lyr} \sim 0.5 \text{ marcsecond}$ . The corresponding cross section is  $2.5 \times 10^{41} \text{ cm}^2 \sim 0''.24^2$ , which is smaller than that of the shock model.

The adiabatic expansion phase plays a crucial role in the X-ray spectral hardening. The synchrotron spectra for  $\Delta r=1.0, 2.0$ , and  $3.0$ , are shown by the thin dotted, dotted-dashed, and dashed lines in Figure 2, respectively, where  $n_e$  is proportional to  $\Delta r^\delta$  due to the shift of the injection energy by the adiabatic expansion. The other model parameters are the same as the fiducial model. We see the spectral hardening is prominent only for  $\Delta r > 2$  and there is no hardening without adiabatic expansion, i.e.  $\Delta r = 1$ . Because  $\gamma_{\text{inj}}$  is fixed, the radio spectrum also changes slightly with  $\Delta r$ . Electron injection from jet to a hotspot AR has long

been debated, the so-called injection problem of shock models (e.g., Carilli et al. 1991). A wide range of  $\gamma_{\text{inj}}$  is used by different authors, e.g.  $\gamma_{\text{inj}} = 10$  used by Croston et al (2005),  $\gamma_{\text{inj}} = 100$  by Carilli et al. (1991), and  $\gamma_{\text{inj}} = 1000$  by Wardle et al. (1998). In the context of SA, an electron energy comparable to the proton rest mass energy is favored because lower energy electrons can be accelerated efficiently by whistler waves (Liu et al. 2006). A recent reanalysis of the BBS of the hotspots in Cygnus A also suggests a sharp spectral break at this energy (Stawarz et al. 2007). We therefore choose  $\gamma_{\text{inj}} = 1800$  for the fiducial model. The two thin solid lines in Figure 2 show the spectra for  $\gamma_{\text{inj}} = 10$ , and 3000. The latter under-predicts the 90 cm radio flux by  $\sim 60\%$ . Here  $n_e \propto \gamma_{\text{inj}}^{-\delta}$  and  $U_e/U_B \propto \gamma_{\text{inj}}^{1-\delta}$ . Figure 2 also shows the spectral evolution assuming a constant injection power and constant magnetic field and electron density in the CR. As expected, the total luminosity of the hotspot increases with time. At  $t = 0.4$  Myr, the X-ray flux is dominated by the SSC component, which may explain the observation that the X-ray emission of high-power hotspots are dominated by SSC (Hardcastle et al. 2004). The SSC component becomes more prominent if a bigger  $U_e/U_B$  is chosen for the fitting, which also results in a lower  $B$ , higher  $\gamma_e$ , and higher energy flux from the AR.

Several models have been proposed for the X-ray spectral hardening before. None of them appears to be applicable to WHPA. We also consider the Klein-Nishina effects of SSC on the electron distribution. Figure 2 shows that the volume of the emission region needs to be at least 10 times smaller than the fiducial model to make the SSC cooling dominant. This leads to an electron to magnetic field energy density ratio greater than  $150^2$  and significant SSC contributions to X-ray emission. The SA itself can also produce hardening near the high energy cutoff (Schlickeiser 1984). However, this is significant only for  $\tau_{\text{esc}} \gg \tau_{\text{ac}}$  ( $\delta \simeq 0$ ). The corresponding electron spectral index is  $\sim 1$ , which is not consistent with observations.

#### 4. Conclusions and Discussion

We have shown that SA reproduces the X-ray spectral hardening of the bright core of WHPA and predicts a spectral cutoff near 1 keV. With few modification, the model can

---

<sup>2</sup>The synchrotron luminosity  $L_{\text{syn}} \propto N_0 R^3 B^2 \gamma_X^2$ , where  $N_0$  is the normalization of the electron distribution and  $\gamma_X$  is the Lorentz factor of electrons producing keV X-rays through synchrotron process, i.e.  $B\gamma_X^2$  is on the order of  $10^{11}$  G. To make the SSC cooling dominant, the energy density of synchrotron photons needs to be greater than the magnetic field energy density, i.e.  $B^2 R^2 < 2L_{\text{syn}}/c$ . The electron energy density is proportional to  $N_0 \gamma_{\text{inj}}^{1-\delta}$ . Then we have  $B^2/N_0 \gamma_{\text{inj}}^{1-\delta} \propto B^4 R^3 \gamma_X^2 / L_{\text{syn}} \gamma_{\text{inj}}^{1-\delta} < 10^{11} (2/c)^{3/2} L_{\text{syn}}^{1/2} \gamma_{\text{inj}}^{\delta-1}$  G. One needs to increase  $\gamma_{\text{inj}}$ , which is constrained by radio flux densities, to bring the magnetic field and electrons close to energy equipartition.

be applied to other *Chandra* X-ray features with similar properties. We emphasize that the shock model has difficulties in explaining these observations since the lifetime of X-ray emitting electrons is too short for the shock to produce the observed high flux levels. This challenges any models with particles accelerated efficiently in very small regions. With a very large shock cross section ( $> 0''.3^2$ ) and high downstream flow velocity ( $> 0.1c$ ), the shock model may fit the BBS of WHPA by assuming a quick adiabatic expansion phase of the downstream flow, similar to the SA model discussed above. However, a power-law spectrum with a photon spectral index of 2.24 is expected beyond the X-ray band except that the acceleration rate of highest energy electrons is fine-tuned to be equal to the cooling rate of X-ray emitting electrons. In this case the model predicted BBS will be indistinguishable from that of the SA model. For Bohm diffusion, the acceleration rate is equal to  $eB\Delta r^2c/2\pi$ , the emission spectrum cuts off at  $\sim 70$  MeV (Blumenthal & Gould 1970). Observations above the *Chandra* band (e.g. with *Suzaku*) can readily distinguish these two models.

The SA is less efficient and operates over an extended region with its size determined by the turbulence generation and decay processes. We predict that the observed harder X-ray emission originates from the AR while the radio (optical) emission comes from the CR. The energy dissipation and the accompanying SA may still be triggered by shock waves. In this case, the traditional study of shock dynamics can be used to make predictions on the displacements between peaks in the X-ray and radio (optical) images. These may explain observations of bright knots in FR I galaxies. The dynamics of jet flows is sophisticated. Some of the energy dissipation regions may not be associated with shock fronts. In this case, one may use MHD simulations to identify regions with strong energy dissipation and apply the SA model to make predictions on the source morphology. MHD simulations may also address the dynamics related to the turbulence and the adiabatic expansion phase introduced to produce the observed spectral hardening.

We thank the referee for careful reading and very helpful comments. This work was supported in part by the NSF of China (grants 10325313, 10733010 and 10521001), CAS key project (KJCX2-YW-T03), the PDF of China (20070410636) and under the auspices of the US Department of Energy by its contract W-7405-ENG-36 to LANL.

## REFERENCES

- Blandford, R. D., & Rees, M. J. 1974, MNRAS, 169, 395  
 Blumenthal, G. R., & Gould, R. J. 1970, RvMP, 42, 237  
 Brunetti, G., Mack, K.-H., Prieto, M. A., & Varano, S. 2003 MNRAS, 345, L40



- Carilli, C. L., Perley, R. A., Dreher, J. W., & Leahy, J. P. 1991, *ApJ*, 383, 554
- Croston, J. H. et al. 2005, *ApJ*, 626, 733
- Dermer, C. D., & Atoyan, A. M. 2002, *ApJ*, 568, L81
- Hardcastle, M. J., Birkinshaw, M., & Worrall, D. M. 2001, *MNRAS*, 326, 1499
- Hardcastle, M. J., Harris, D. E., Worrall, D. M., & Birkinshaw, M. 2004, *ApJ*, 612, 729
- Hardcastle, M. J., Croston, J. H., & Kraft, R. P. 2007a, *ApJ*, 669, 893
- Hardcastle, M. J. et al. 2007b, *ApJ*, 670, L81
- Harris, D. E., Mossman, A. E., & Walker, R. C. 2004, *ApJ*, 615, 161
- Heavens, A.F., & Meisenheimer, K. 1987, *MNRAS*, 225, 335
- Kronberg, P. P., Colgate, S. A., Li, H., & Dufton, Q. W. 2004, *ApJ*, 604, L77
- Liu, S. M., Melia, F., & Petrosian, V. 2006, *ApJ*, 636, 798
- Liu, S. M., Melia, F., Petrosian, V., & Fatuzzo, M. 2006, *ApJ*, 647, 1099
- Marshall, H. L. et al. 2002, *ApJ*, 564, 683
- Meisenheimer, K. et al. 1989, *A&A*, 219, 63
- Meisenheimer, K., Yates, M. G., & Roeser, H.-J. 1997, *A&A*, 325, 57
- Migliori, G. et al. 2007, *ApJ*, 668, 203
- Park, B. T., & Petrosian, V. 1995, *ApJ*, 446, 699
- Perley, R. A., Röser, H.-J., & Meisenheimer, K. 1997, *A&A*, 328, 12
- Petrosian, V., & Liu, S. M. 2004, *ApJ*, 610, 550
- Sambruna, R. M., et al. 2004, *A&A*, 414, 885
- Schlickeiser, R. 1984, *A&A*, 136, 227
- Spergel et al. 2003, *ApJS*, 148, 175
- Schwartz, D. A, et al. 2000, *ApJ*, 540, L69
- Stawarz, L., Cheung, C. C., Harris, D. E., & Ostrowski, M. 2007, *ApJ*, 662, 213

Wardle, J. F. C., Homan, D. C., Ojha, R., & Roberts, D. H. 1998, *Nature*, 395, 457

———. 2001, *ApJ*, 547, 740

Wilson, A. S., & Young, A. J. 2002, *ApJ*, 568, 133

Worrall, D. M., Birkinshaw, M., & Hasdcastle, M. J. 2001, *MNRAS*, 326, L7

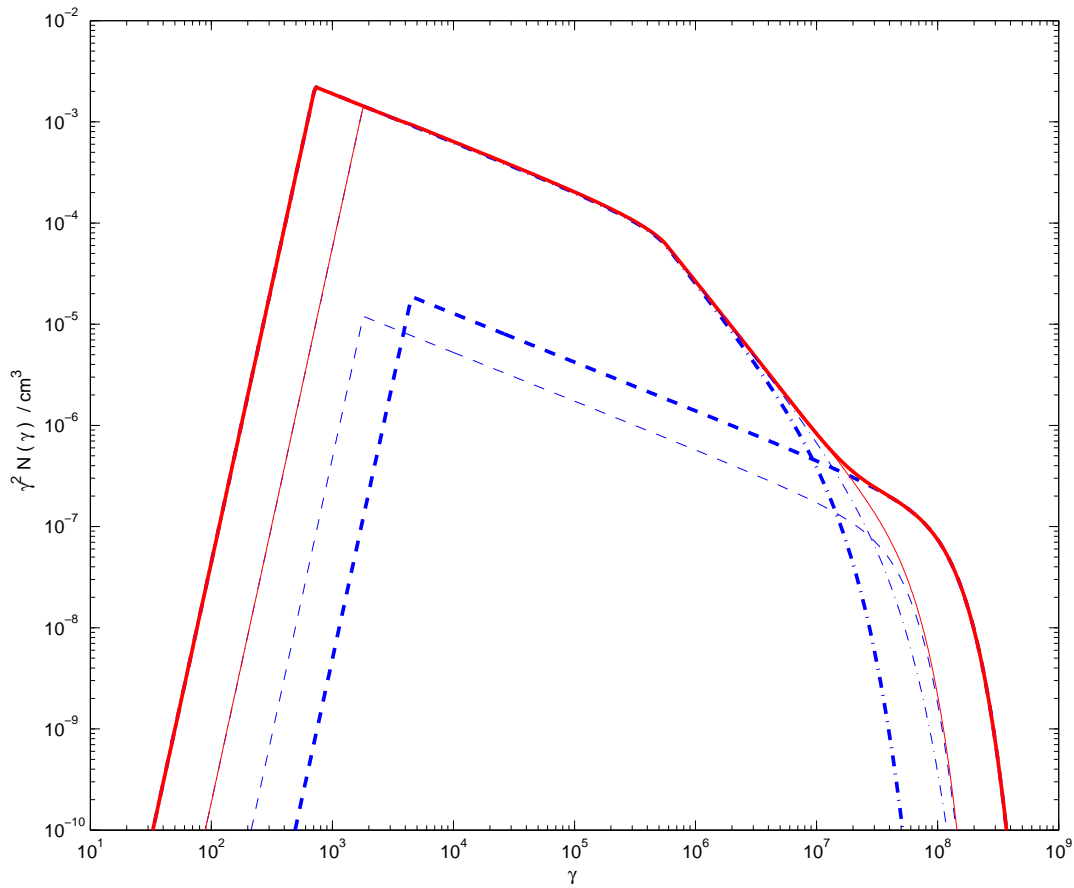


Fig. 1.— Effective electron distributions for  $\Delta r = 2.5$  (thick) and  $1.0$  (thin). The dashed and dotted-dashed lines are for the acceleration and CR, respectively. The solid lines are the sums of the two. The normalization is for the fiducial model. See text for the rest of the model parameters.

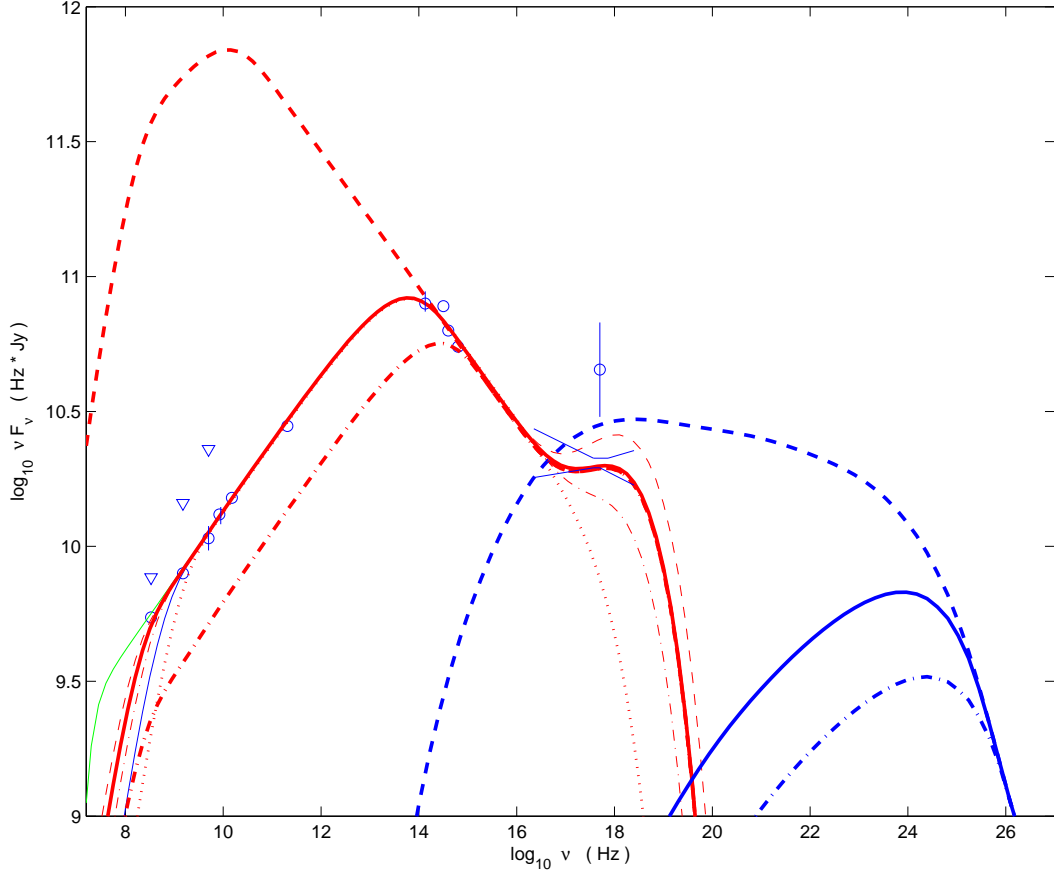


Fig. 2.— Best fit to the spectrum of WHPA and effects of  $\Delta r$ ,  $\gamma_{\text{inj}}$ , and  $t$ . The data are from Wilson, Young & Shopbell (2001). The thick solid line is the best fit with  $\Delta r = 2.5$ ,  $B = 85 \mu\text{G}$ ,  $n_e = 2.8 \times 10^{-6} \text{cm}^{-3}$ , and  $t = 5.2 \text{ kyr}$ . The thin dashed, dotted-dashed, dotted lines are for  $\Delta r = 3.0, 2.0, 1.0$ , respectively. The two thin solid lines are for  $\gamma_{\text{inj}} = 3000$ , and 10 with the former having a lower radio flux. The downward triangle radio points are for spatially unresolved fluxes from Perley, Röser & Meisenheimer (1997). Their relatively harder spectrum suggests a spectral break near  $\gamma \sim 1000$ . The higher energy components are produced through SSC. The thick dotted-dashed and dashed lines are for  $t = 2.3$  and 400 kyr, respectively. The SSC component dominates the X-ray flux for the latter.